PHYSICS RESEARCH AND TECHNOLOGY

THE ORIGIN OF GRAVITY FROM FIRST PRINCIPLES

Volodymyr Krasnoholovets
Editor

NOVA

V. Krasnoholovets, Derivation of gravity from first submicroscopic principles, in *The Origin of Gravity from First Principles*, Ed.: V. Krasnoholovets, Nova Science Publishers, Inc. (2021), pp. 281-332

Chapter

DERIVATION OF GRAVITY FROM FIRST SUBMICROSCOPIC PRINCIPLES

Volodymyr Krasnoholovets*

Department of Theoretical Physics,
Institute of Physics, Kyiv, Ukraine

ABSTRACT

A submicroscopic theory of real physical space is outlined, showing that space is constituted as a mathematical lattice of primary topological balls, known as the tessellattice. The main parameter – mass – is introduced as a local fractal volumetric deformation of a cell of the tessellattice. Due to the interaction with ongoing cells of the tessellattice, a moving particle is desintagrated to a cloud of spatial excitations named *inertons*. So, the moving particle together with its inerton cloud is mapped to the quantum mechanical formalism as a particle's wave ψ-function. Inertons oscillating around a massive object behave like standing spherical waves and establish a peculiar landscape in the tessellatice around the object. In the mean-field approximation the landscape looks like Newton's gravitational potential $-Gm/r$. The tangential movement of a test object creates an additional term to

* Corresponding Author's Email: krasnoh@iop.kiev.ua.

Newton's gravity proportional to v_{tang}^2 / c^2. Such a submicroscopic gravitational potential allows one to solve all the problems predicted by the phenomenological theory of general relativity and also shows how inerton physics can work out a number of new problems, in particular the emission of new unknown radiation from the Sun. Arguments are given in favor of introducing a new branch of astrophysics – inerton astronomy.

Keywords: space, tessellattice, fractals, mass, inertons, gravity

INTRODUCTION

Textbooks of physics inform us that gravity is a force that makes things move towards each other and that gravitational theories deal with attraction of massive bodies. According to Newton, objects are attracted through the gravitational force. In Einstein-Hilbert theory, gravitation arises from the warping of space and time, such that a curvature instead of a force appears around a massive body. This implies that the curvature of space-time and the absence of the force of attraction radically violate Newton's theory. Nevertheless, the first term in general relativity is Newton's potential – Gm/r (see e.g., Bergmann, 1976), despite the fact that the origin of Newton's force is unclear. General relativity suggests that matter bends space-time and in turn the bending creates a peculiar force that acts on the object under consideration. That is, the force appears because the object follows its geodesic path through space-time. Hence a landscape described by the object's geodesic path plays the role of the source of attraction.

Two difficult problems remain unsolved. The first problem relates to the behavior of gravity at scales close to the particle's de Broglie wavelength, where quantum mechanical laws start to become relevant. This includes smaller length scales which lay behind the quantum mechanical formalism. In other words, how does gravity arise for microscopic systems?

The second problem concerns the definition of mass. In fact, the current framework of physics does not offer a rigorous definition of mass. This further inhibits our first-principle based understanding of gravity.

We must begin by defining the concept of mass, because it is a mass m that bends the ambient space (or space-time). An exact formulation can be given only in terms of a physical theory that is beyond the quantum mechanical formalism, because the modern theory of quantum physics does not offer a self-consistent definition of mass. Attempting to do so from a quantum-mechanical perspective, we find ourselves in an unknowable world that is inaccessible even to the intricate formal methods of physical mathematics, which actively promotes an abstract discipline known as quantum gravity developed mainly on the bifurcated foundations of strings and loops.

THE NOTION OF MASS

It is evident that the physics of deep space must have its own nuances. In the 1860s and 1870s, Bernhard Riemann and Hermann von Helmholtz, when considering the movement of an object through space, noted that although the space around the object is curved, the object itself remains 'rigid.' In other words, they defined the first essential feature that distinguishes an object from space: the moving object has to be 'rigid' and the space has to be 'soft.'

Clifford (1882) considered the creation of matter and its movement as the appearance of curvature of local pieces of space, which occurred in four stages: 1) small curved portions of space could be treated as matter because the ordinary laws of geometry are not valid in them; 2) a curved/distorted property could travel from one portion of space to another, like a wave; 3) this variation of curvature happens in the motion of matter; 4) in the physical world only this variation occurs.

Michel Bounias (1990; Bounias and Krasnoholovets, 2003) suggested the constitution of physical space as something that initially consisted of objects and intervals. That is, it appears that from the mathematical point

of view a solid itself is an element of space, and because of that a moving solid has to be considered as part of that space as well. An analogy can be made with water and ice. Although ice cubes float in water, they nevertheless remain water, but are in a different physical state.

Set theory, fractal geometry and topology allowed us (Bounias and Krasnoholovets, 2003) to contruct the real physical space as a mathematical lattice of primary topological balls. Such a lattice was named the *tessellattice* by M. Bounias; topological balls play the role of cells in the tesellatice. The tessellattice is empty if no deformations are available. But what types of deformations can exist in the tessellattice? In general they are:

- a contraction of the cell;
- an inflation of the cell;
- a shift of the cell from its equilibrium position.

Furthermore, the tessellattice as a whole should possess elastic properties, since it is a substrate.

We have been talking about primary topological balls whose dense lattice forms the tessellatice, thereby making up the inner structure of ordinary physical space. But what could be the size of such a ball, or cell, in the tessellattice? Logically, the size of a ball in a degenerate state can be related to the Planck length $l_{\mathrm{P}} = \sqrt{\hbar G / c^3} \simeq 1.616 \times 10^{-35}$ m.

Our studies have shown that contractions and inflations of a cell could not be stable if they occured without changes of homeomorphism (Figure 1a). A morphism with a dimensional change, which occurs upon infinitely repeated iteration, forms a stable local deformation in the cell under consideration (Figure 1b).

A stable local deformation can be presented as a convoluted product of 3D space coordinates, which results in the appearance of an embedding D4 part as below

$$\mathrm{D4} = \int \left(\int_{dS} d\vec{x}\, d\vec{y}\, d\vec{z} \right) * d\Psi(w) \tag{1}$$

where dS is an element of space-time and $d\Psi(w)$ is a function accounting for the extension of 3D coordinates to the fourth dimension through convolution ($*$) with the volume of space. In such a way, the local deformation with dimensionality 3D + δD ≤ 4D formed by means of volumetric fractal iterations becomes a rigid object in the unmanifested space. Hence a cell with such deformation is different from any other degenerate cell of the tessellattice (i.e., the unmanifested real physical space) and the objective characteristic of such difference is a ratio (3D + δD)/3D > 1.

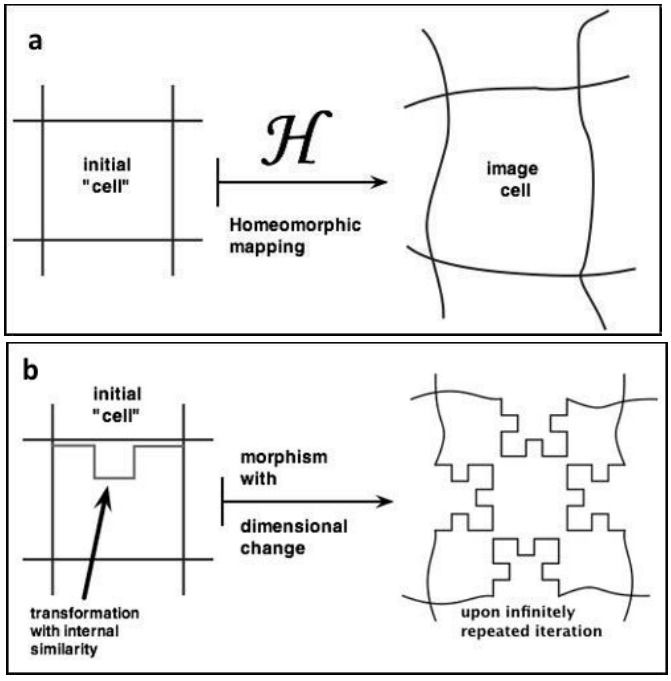

Figure 1. Homeomorphic variation (a) and dimensional change (b) of a cell in the tessellattice.

In Figure 1b, at the *i*th iteration corresponding subvolumes ($\mathcal{V}_i$) depend on the subvolumes of the previous iteration, which in the simplest case are related as $\mathcal{V}_i = \mathcal{V}_{i-1} \cdot (1/r_0)^3$ where r_0 is the characteristic linear size of a degenerate cell. The total volume occupied by the subvolumes formed by fractal iteration to infinity is the sum of the series

$$\mathcal{V}^{\text{frac}} = \sum_{i=1\to k} \left((r_0 + \delta r)^i \cdot \mathcal{V}_{i-1} \cdot (1/r_0)^3 \right), \tag{2}$$

which means that a fractal decomposition consists in the distribution of the members of the set of fractal subfigures. These subfigures are constructed on the primary cell and are similar to it.

The deformed ball as considered above provides a formalism describing the elementary particles. It follows that mass is represented by a fractal reduction of the volume of a ball. If $\mathcal{V}^{\text{deg}}$ is the volume of a cell in the tessellattice (the degenerate state of a ball), then the reduction of volume resulting from a fractal concavity is $\mathcal{V}^{\text{particle}} = \mathcal{V}^{\text{deg}} - \mathcal{V}^{\text{frac}} = \Delta\mathcal{V} > 1$, or in line with expression (2)

$$\mathcal{V}^{\text{particle}} = \mathcal{V}^{\text{deg}} \times \left\{ 1 - \sum_i \left((r_0 + \delta r)^i \cdot \mathcal{V}_{i-1} \cdot (1/r_0)^3 \right) \right\}. \tag{3}$$

Now we can introduce the notion of mass m_B of a particled ball *B* as a function of the fractal-mediated decrease of the volume of the ball, i.e.,

$$\begin{aligned} m_B &= C \cdot \mathcal{V}^{\text{deg}} / \mathcal{V}^{\text{particle}} \times \left\{ 1 - \sum_i \left((r_0 + \delta r)^i \cdot \mathcal{V}_{i-1} \cdot (1/r_0)^3 \right) \right\}^{-1} \\ &= C \cdot \mathcal{V}^{\text{deg}} / \mathcal{V}^{\text{particle}} \cdot (e_V - 1)_{e_v \geq 1} \end{aligned} \tag{4}$$

where (e) is the Bouligand exponent and $(e_V - 1)$ depicts the gain in dimensionality given by the fractal iteration. Here, $\mathcal{V}^{\deg} > \mathcal{V}^{\text{particle}}$ and $(e_V - 1)$ is positive and even more, $(e_V - 1) > 1$. This means that the right hand side of expression (4) is positive and greater than unity; C is a dimensional constant.

Thus, expression (4) defines the physical concept of mass from first principles.

DECOMPOSITION OF THE PARTICLE MASS TO INERTONS

Since a particle is created in the environment of other similar cells, they have to react to its structure. If the particle is contracted following the law of fractal iterations, the surrounding cells must be stretched, that is, they must have a tension that keeps them in a tense state. Gradually, the tension of surrounding cells must decrease, and the entire tense region has to be characterized by a certain radius $\lambda_{\text{Com}}/2$. Here λ_{Com} represents the Compton radius of the particle in question. The behavior of cells in this region, also known as the deformation coat (Krasnoholovets, 2017), obeys the Klein-Gordon equation (Christianto et al., 2019). The space beyond this region is the usual degenerate tessellattice.

When the particle starts to move it must interact with neighbouring cells of the surrounding space. This movement implies an ongoing exchange of properties between mass and tension: step by step, the particle loses its fractals (i.e., fragments of mass) and passes them on to the neighbouring cells, and on their turn the cells pass their tension to the moving particle. Hence a cloud of spatial excitations appears around the moving particle. These excitations carry fragments of mass; they were termed *inertons* (Krasnoholovets, 2017) because they represent the force of inertia and appear owing to the resistance of the physical space (the tessellattice) to the movement of an object.

As excitations of physical space, inertons migrate by a relay mechanism hopping from cell to cell, while the particle itself moves by squeezing itself between cells of the tessellattice.

Since the moving particle loses its mass and momentum (and it's velocity) due to scattering with ongoing cells, it must eventually stop. The section in which the particle emits all its mass through inertons corresponds to its de Broglie wavelength $\lambda_{\rm dB}$. This region demonstrates the submicroscopic dynamics of the particle (Krasnoholovets, 2017). After passing the section $\lambda_{\rm dB}$ the particle loses its mass and becomes massless; however, it acquires a tension $\vec{\xi}$ that coincides with the initial velocity vector of the particle. The motion of the particle's inertons shows that they migrate through the tessellattice in the direction transversal to the particle path, up to the distance $\Lambda = \lambda_{\rm dB} c / \upsilon$. This distance Λ can be termed the amplitude of the particle's inerton cloud. Here, c represents the sound velocity of the tessellattice, also known as the speed of light, and υ is the initial velocity of the particle. It should be noted that in the tessellattice, the longitudinal speed of sound $\hat{c}$ (the speed of free inertons) may exceed the transverse speed of sound c (the speed of light); a preliminary estimate is $\hat{c} \sim 100 c$ (Krasnoholovets and Tane, 2004).

What happens to an inerton when it reaches the distance Λ? The cell to which the inerton has arrived becomes shifted from its equilibrium position in the direction away from the particle. At this point the inerton stops – its velocity becomes zero but the tension in the cell reaches its maximum value. Due to the elasticity of the tessellattice, the cell is pushed back to its equlibrium position. This causes the tessellattice to launch the inerton back to the moving particle, which caused the excitation. While arriving back to the particle following a speed-dependent potential, the inerton loses the tension $\vec{\xi}$ and gains its mass μ. Upon arrival, the inerton passes the particle mass fragment μ back to the particle, thereby restoring its original mass.

The oscillating inerton motion is described by the equation

$$\mu d^2\vec{\chi}/dt^2 = -\gamma\vec{\chi} \tag{5}$$

where $\vec{\chi}$ is the coordinate of the inerton and γ is the elasticity constant of the tessellattice. The equation shows that the initial kinetic energy of the inerton, when it is emitted by the particle $\mu\dot{\vec{\chi}}^2/2|_{\dot{\chi}=c} = \mu c^2/2$, passes to the potential energy $\gamma\omega^2\Lambda^2/2$ at the point $|\vec{\chi}\|_{\max} = \Lambda$, before being returned again to $\mu c^2/2$ and undergoing further mass-tension cycles. Here, the cyclic frequency is given by the elasticity of the tessellattice, which guides the inerton, and the inerton mass μ (i.e., the degree of volumetric fractal contraction of the cell): $\omega = \sqrt{\gamma/\mu}$.

To show the migrational transformation of the inerton from mass to tension state, we have to construct the appropriate Lagrangian which includes both mass and tension terms, as well as a term accounting for the interaction of both states:

$$L = \tfrac{1}{2}\lambda^2\dot{\mu}^2 + \tfrac{1}{2}\mu_0^2\dot{\vec{\xi}}^2 + c\mu_0\lambda\dot{\mu}\vec{\nabla}\vec{\xi}\,. \tag{6}$$

Here, the variables $\mu(\vec{\chi}, t)$ and $\vec{\xi}(\vec{\chi}, t)$ characterize the mass and tension of the inerton, respectively; λ is the characteristic inerton wavelength (the de Broglie wavelength in the case of a particle); μ_0 is the initial mass of the inerton and v the initial velocity of the particle. Since the Lagrangian (6) contains the term $\vec{\nabla}\vec{\xi}$, the Euler-Lagrange equations for variables μ and $\vec{\xi}$ are (ter Haar, 1974)

$$\frac{\partial}{\partial t}\left(\frac{\partial L}{\partial \dot{Q}}\right) - \frac{\delta L}{\delta Q} = 0\,,$$

$$\frac{\delta L}{\delta Q} = \frac{\partial L}{\partial Q} - \frac{\partial}{\partial x}\frac{\partial L}{\partial(\partial Q/\partial x)} - \frac{\partial}{\partial y}\frac{\partial L}{\partial(\partial Q/\partial y)} - \frac{\partial}{\partial z}\frac{\partial L}{\partial(\partial Q/\partial z)}$$

(where $Q \equiv \mu, \vec{\xi}$), which leads us to the following differential equations in explicit form

$$\mu_0^2 \ddot{\vec{\xi}} + c\mu_0 \lambda \vec{\nabla} \dot{\mu} = 0, \quad \lambda \ddot{\mu} + c\mu_0 \lambda \vec{\nabla} \dot{\vec{\xi}} = 0. \tag{7}$$

From these equations we obtain the typical wave equations of motion for each of the two variables

$$\ddot{\mu} - c^2 \nabla^2 \mu = 0, \quad \ddot{\vec{\xi}} - c^2 \nabla^2 \vec{\xi} = 0. \tag{8}$$

Therefore, the equations for the variation of the mass μ and tension $\vec{\xi}$, which move in antiphase, show that an inerton moves as a typical wave. Stated otherwise, the fractal contraction of a cell (the mass μ) is periodically replaced by the stretching of the cell (the tension $\vec{\xi}$).

The wave equations (8) allow two different solutions, corresponding to a standing and a travelling wave.

For inertons which are emitted by a moving particle and then reabsorbed by the particle after reflection from a distant point Λ of the tessellattice, their trajectories look like strings attached to the point-particle. That is why formally, the appropriate solutions for the inerton mass and tension could look as follows

$$\mu(\vec{\chi}, t) = \mu_0 \cos(\vec{k}\vec{\chi}) \cos(\omega t), \tag{9}$$

$$\vec{\xi}(\vec{\chi}, t) = \vec{\xi} \sin(\vec{k}\vec{\chi}) \sin(\omega t) \tag{10}$$

where the wave number $k = 2\pi/(2\Lambda)$ and the cycle frequency $\omega = 2\pi/(2T)$. Here, Λ is half of the spatial period (amplitude) of the oscillating inertons and T is half of the period of the standing inerton wave. At the point $|\vec{\chi}| = 0$, which is associated with the position of the particle,

the inerton mass is μ_0; at the maximum distant point $|\vec{\chi}| = \Lambda$ the inerton mass becomes 0. The tension oscillates in antiphase to the mass: at the point $|\vec{\chi}| = 0$ the tension is 0 and at the point $|\vec{\chi}| = \Lambda$ the tension becomes $\vec{\xi}_{\max}$.

The solutions (9) and (10) assume the validity of the dispersion relation $\omega = ck$.

The traveling wave solutions of equations (8) can then be written as

$$\mu(\vec{\chi},\ t) = \mu_0\left[1+\cos(\vec{k}\vec{x}-\omega t)\right], \tag{11}$$

$$\vec{\xi}(\vec{\chi},\ t) = \vec{\xi}_{\max}\left[1+\cos(\vec{k}\vec{x}-\omega t)\right]. \tag{12}$$

The solutions (11) and (12) describe the migration of a free inerton released from the particle's inerton cloud. The small local contraction (the mass μ) and the corresponding small local stretching (the tension $\vec{\xi}$) are two opposite features of the inerton. The wave number $k = 2\pi/\lambda$ of the free inerton is defined by its wavelegth λ that has been imparted upon it at the moment of release from the particle's inerton cloud. The same holds for the cyclic frequency $\omega = 2\pi/T$ in which T is the period defined by the relationship $c = \Lambda/T$.

To summarize, we have considered how particle mass is decomposed to inertons and illustrated their characteristic properties, concluding that inertons exhibit wave attributes typical for waves in elastic condensed matter systems.

THE STANDING SPHERICAL INERTON WAVE

In the previous section we have examined the behavior of inertons from a particle's inerton cloud and showed that their motion can formally be described by a standing wave with solutions (9) and (10). Let us now

consider the emission of such inertons in more detail. We start by fixing the frame of reference to the particle, so that the particle is stationary in the corresponding coordinate system (its velocity $\vec{v} \equiv 0$). In this reference frame, the particle emits inertons in a sphere, and the inertons reaching the boundary located at a distance $r = \Lambda$ are reflected back to the particle (Figure 2). The emission of inertons in the sphere occurs sequentially, starting with the 1st shell, followed by the 2nd shell, and so forth, up until the N^{th} shell. In addition to this, an order of emission is postulated – the inerton cloud unfolds like a spiral, which is caused by surface fractals that characterize the electric and magnetic properties of the particle cell (Krasnoholovets, 2017; 2019). In Figure 2, the spiral develops counter-clockwise.

Thus, inertons oscillate from the central point to the boundary of the sphere distant by Λ from the center. This means that the problem of oscillation of inertons can be reduced to the problem of radial vibrations of a gas in a sphere (Koshlyakov et al., 1970). As it follows from Euler's hydrodynamics, sound waves in ideal liquids and gases are longitudinal, which makes it possibe to describe them using a single scalar potential φ called the velocity potential. Then the vibrational speed is expressed in the form $\vec{u} = \vec{\nabla}\varphi$. The velocity potential satisfies the wave equation (see expressions (8)). The oscillating behavior of the radial velocity potential u and the variables m and ξ coincides because of the same initial and boundary conditions, which for our case of inertons are:

$$\begin{aligned} &\mu\big|_{t=0} = \mu(r), \quad \partial\mu/\partial t\big|_{t=0} = F(r), \quad \xi\big|_{t=0} = \xi(r), \quad \partial\xi/\partial t\big|_{t=0} = \Phi(r), \\ &\partial\mu/\partial r\big|_{r=\Lambda} = 0, \quad \partial\xi/\partial r\big|_{r=\Lambda} = 0. \end{aligned} \tag{13}$$

Using the expression for the Laplace operator in spherical coordinates we can rewrite the wave equations (8) in the form

$$\frac{\partial^2 u}{\partial r^2} + \frac{2}{r}\frac{\partial u}{\partial r} = \frac{1}{c^2}\frac{\partial^2 u}{\partial t^2}. \tag{14}$$

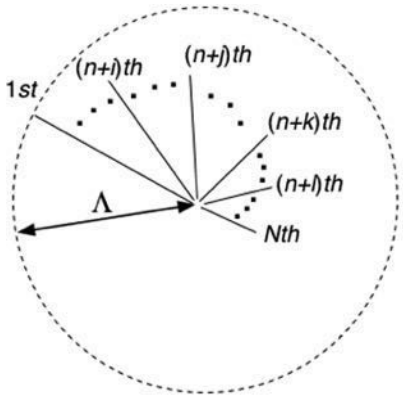

Figure 2. Spherical oscillations of inertons around a particle.

Partial solutions are sought in the form $u(r,\, t) = w(r)T(t)$ and the equations become

$$w''(r) + \frac{2}{r}w'(r) + k^2 w(r) = 0\,, \tag{15}$$

$$T''(t) + k^2 c^2 T(t) = 0\,. \tag{16}$$

The general solutions to Eqs. (15) and (16) are, respectively

$$w(r) = C_1 \frac{|\sin kr|}{r} + C_2 \frac{|\cos kr|}{r}\,. \tag{17}$$

$$T(t) = C_{11}\,|\sin(\omega t)| + C_{22}\,|\cos(\omega t)|\,, \tag{18}$$

where $\omega = kc$. The modulus sign is needed because the values of mass and tension cannot be negative.

Based on the initial and boundary conditions (13) and the conditions that at the point $r = 0$ the mass of the ith inerton is $\mu\,|_{r=0} = \mu_0$ and its tension is $\xi\,|_{r=0} = 0$, and at the point $r = \Lambda$ the mass of an inerton is

$\mu|_{r=\Lambda_i}=0$ and its tension is $\xi|_{r=\Lambda_i}=\xi_{\max,\,i}$, we finally obtain the solutions for the interton amplitudes of mass μ_i and tension ξ_i:

$$\mu_i(r,\,t)=\mu_0\frac{r_{01}}{r}\left|\cos\left(\frac{2\pi r}{\Lambda_i}\right)\right|, \tag{19}$$

$$\xi_i(r,\,t)=\xi_{\max,\,i}\frac{\Lambda}{r}\left|\sin\left(\frac{2\pi r}{\Lambda_i}\right)\right| \tag{20}$$

where the minium value of r is even less than the size of a cell, i.e., Planck's length; r is limited by the constant r_{01} (Krasnoholovets, 2017; p. 350): the minimal length of the quantum motion of the particle is its Compton wavelength λ_{Com}; the number of inertons emitted by the particle while passing its Compton wavelength is $\lambda_{\text{Com}}/l_{\text{P}}\approx 10^{20}$, and the constant becomes $r_{01}=l_{\text{P}}/(\lambda_{\text{Com}}/l_{\text{P}})\approx 10^{-55}$ m. Here $k_i=2\pi/\Lambda_i$, $\Lambda_i=\lambda_{\text{dB}}\,c/\upsilon_i$ and $i=1,\,2,\,...,\,N/2\sim 10^{25}$. Recall that the particle velocity reduces gradully from $\vec{\upsilon}$ to zero in the section λ_{dB} due to collisions with ongoing cells of the tessellattice, resulting in emission of approximately 10^{25} inertons.

The solutions for the entire inerton cloud look as follows:

$$m(r,\,t)=m_0\frac{r_{01}}{r}\left|\cos\left(\frac{2\pi r}{\Lambda}\right)\right|\left|\cos\left(\frac{2\pi t}{T}\right)\right|, \tag{21}$$

$$\Xi(r,\,t)=\Xi_{\max}\frac{\Lambda}{r}\left|\sin\left(\frac{2\pi r}{\Lambda}\right)\right|\left|\sin\left(\frac{2\pi t}{T}\right)\right|. \tag{22}$$

These solutions show that the mass of any massive particle is distrubuted around it as a standing sperical wave. Such a distribution occurs in the interior of a sphere with radius Λ. The radius Λ describes the limit to which the quantum mechanical formalism is applicable; beyond Λ the macroscopic world starts, and quantum-mechanical rules transform to the rules of classical physics. In other words, the particle with its inerton cloud is mapping to the qunatum mechnical formalism as the particle's wave ψ-function.. In this context, a force in space can be described as arising during a length equal to the particle's de Broglie length λ_{dB}, and reaching up to the amplitude of particle's inerton cloud $\Lambda = \lambda_{\text{dB}}\, c / \upsilon$. The de Broglie wavelength λ_{dB} of an electron in an atom is 10^{-10} m, hence $\Lambda \sim 100\,\lambda_{\text{dB}} \sim 10^{-8}$ m. Thus Λ determines the distance to which the gravitational interaction of the particle under consideration is able to propagate.

NEWTON'S LAW OF GRAVITAION

Newton's physics is the physics of the macroscopic world. Hence we have to move from considering a single massive particle to considering an ensemble of massive particles. A typical case is represented by a solid in which atoms are packed in a crystal lattice. In the lattice, atoms oscillate near their equilibrium positions. Any motion of a material object is accompanied by the appropriate motion of its inerton cloud (Krasnoholovets, 2017), and in a solid object the inerton clouds of neighbouring atoms overlap.

The spectrum of acoustic waves can be presented in the form of $\lambda_n = 2\,g\,n$ where g is the lattice constant; $n = 1,\ 2,\ \ldots\ N/2$ and N is the number of entities (i.e., atoms) in the solid under consideration. Then the fundamental wavelegth is $\lambda_N = g\,N$. In 1 cm^3 of a solid there are about 10^{22} atoms. Then the fundamental wavelength for this piece of matter is

$\lambda_{\text{fund}} \sim 10^{12}$ m. The corresponding de Broglie wavelegth for this fundamental acoustic excitation becomes $\Lambda_{\text{fund}} = \lambda_{\text{fund}}\, c/\upsilon \sim 10^{18}$ m. In 1 m^3 of a solid there are about 10^{28} atoms, then $\lambda_{\text{fund}} \sim 10^{18}$ m and $\Lambda_{\text{fund}} = \lambda_{\text{fund}}\, c/\upsilon \sim 10^{24}$ m, which is already approaching the visible radius of the Universe. In other words, Λ_{fund} is the amplitude of the object's inerton cloud and its extent is enourmous.

The object's inerton cloud oscillates in such a way that the mass and tension change in the radial direction following the laws (21) and (22). Let us conider the behavior of the standing massive variable $m(r,t)$:

$$m(r,\, t) = m_0 \frac{r_{01}}{r} \left| \cos\left(\frac{2\pi r}{\Lambda_{\text{fund}}} \right) \right| \left| \cos\left(\frac{2\pi t}{T_{\text{fund}}} \right) \right|, \tag{23}$$

where m_0 is the mass of the macrocopic object in question, and r is the distance from the object to the front of the object's inerton cloud. We assume the dispersion law $c = \Lambda_{\text{fund}} / T_{\text{fund}}$ holds in the cloud. Since any real distance $r << \Lambda_{\text{fund}}$ and also $t << T_{\text{fund}}$ we immediately get from the expression (23) a mean field approximation

$$m(r,\, t) \simeq m_0 \frac{r_{01}}{r}\,. \tag{24}$$

Note that in the mean field approximtion a short-distance action is averaged out and only actions at a distance remain.

The solution (24) shows that the mass m_0 of an object exhibits a stationary distribution in the surrounding space. Here it is helpful to recall that mass has been defined as a volumetric fractal contraction of a cell. Hence the distribution (24) reflects the contraction of ambient space around the massive object – the mass distribution decreases along the

radial line as $1/r$ from the object to the boundary of the inerton cloud, meaning the contraction of cells decreases towards the boundary of the inerton cloud.

The tension $\vec{\xi}$ is practically constant near the object while $r << \Lambda_{\text{fund}}$ and remains equal to zero. That is why we can only pay attention to the distribution of quasi-local deformations (i.e., mass in the physical terms) around the object as the expression (24) prescribes.

The potential energy of the gravitational interaction between two massive objects with masses m_1 and m_2 can be written in a way similar to that presented for the interaction of quarks and nucleons (Krasnoholovets, 2017; p. 351),

$$U = -\frac{m_1}{m_{\text{P}}}\frac{m_2}{m_{\text{P}}}\frac{hc}{r} \tag{25}$$

where m_{P} is the Planck mass, i.e., the maximum possible volumetric deformation of a cell in the tessellattice. The expression (25) can be written in the standard form via the phenomenological gravitational constant G:

$$U = -G\frac{m_1 m_2}{r}, \tag{26}$$

which is the well-known Newtonian potential energy related to the gravitational interaction of two bodies with masses m_1 and m_2.

To summarize, the phenomenon of gravity experienced by a small mass m_2 in relation to a large mass m_1 is caused by the landscape induced by the mass m_1 in the ambient space: the potential $-Gm_1/r$ allows the mass m_2 to descend along the radially symmetric landscape induced by the standing inerton wave of the central mass m_1. The standing inerton cloud

of the central mass m_1 is imposed by the overlap of individual inerton clouds of the atoms making up the object m_1. This perspective does not include any curvature of space-time. The landscape formed by the fundamental standing inerton wave induces a potential force of attraction, drawing in a smaller mass m_2 along the deformation field created by the larger mass m_1.

AN IMPORTANT CORRECTION TO NEWTON'S GRAVITY

In the preceding sections, we have seen that a local deformation δm does not create a curvature in the tessellattice, even though cells around the deformation become partly stretched. By definition (1) the local deformation is a convoluted product of 3D spatial coordinates, which generate an embedding 4D part. Mass is defined through expression (4). Hence, no curvature shall appear in the ambient space around δm, meaning that in terms of general relativity the Newton metric is flat.

However, general relativity states that a metric of a massive point is curved at the macroscopic scale. Let us clarify this situation by showing when a curvature actually appears.

It is obvious that a certain perturbation has to pop up to warp the ambient space. Possibly, it relates to a test mass that emerges in the gravitational field of the mass m_1 under study?

A small test mass m_2 possessing a tangential velocity $\vec{v}_\perp$ may appear in the vicinity of the large mass m_1 (Figure 3). The mass m_2 is charcterized by its own inerton cloud. The extent of this inerton cloud is very long, which means that the inerton cloud of the orbital mass m_2 overlaps with the central mass m_1. Therefore, through their inerton clouds, the interaction between these two masses is established. The velocity components of the satellite's inerton cloud are $\vec{c}$ along the radial line

(Figure 3) and $\vec{v}_{\perp}$ along the tangential direction. Due to the two velocity components of the satellite, it falls towards the mass m_2, not to the central point located at $\vec{r}$, but to the point $\vec{r}'$ (Figure 3). The total velocity of inertons in the satellite's inerton cloud, which travel to this point, is $c_+ = \sqrt{\vec{c}^2 + \vec{v}_{\perp}^2}$.

Recall that Poincaré (1906; 1908) referring to Laplace noted that the force causing the attraction of a body depends on the position and velocity of the body, and that the mass as a coefficient of attraction depends on the velocity. He further pointed to the fact that if the body in question has a velocity, then the resultant force of attraction between two bodies is not directed along the straight line joining the two bodies, so that the resultant force should have a small angle of deviation from the direct line.

Hence owing to the tangential velocity $\vec{v}_{\perp}$ the satellite's inertons arrive to the point $\vec{r}'$ faster than they can travel to the point $\vec{r}$ when the tangential velocity is absent, i.e., when $\vec{v}_{\perp} = 0$. These inertons arrive to point $\vec{r}'$ in time $t' = t / \sqrt{1 + \vec{v}_{\perp}^2 / \vec{c}^2}$, with the path given by $r' = r / \sqrt{1 + \vec{v}_{\perp}^2 / \vec{c}^2}$.

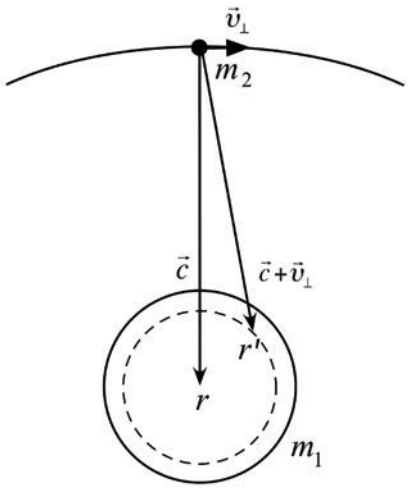

Figure 3. Test mass m_2 in the vicinity of the large mass m_1.

Formally using the Minkowski metric developed in an abstract empty space we can write the square form for a linear element ds in the point $\vec{r}$ as below

$$ds^2 = c^2 dt^2 - d\vec{r}^2 \tag{27}$$

where time t plays the role of a natural parameter, i.e., $\int c\,dt = l$. In the other reference frame for point $\vec{r}'$, we have

$$ds'^2 = c^2 dt'^2 - d\vec{r}'^2 . \tag{28}$$

Equating the squares of the linear forms (27) and (28) to zero, namely, putting $ds^2 = ds'^2 = 0$, we get the equation

$$c^2 dt^2 - d\vec{r}^2 = c^2 dt'^2 - d\vec{r}'^2 \tag{29}$$

and by allowing the shortening of time dt' (i.e., $dt' = dt / \sqrt{1 + \vec{v}_\perp^2 / \vec{c}^2}$), we obtain

$$dr'^2 = dr^2 / (1 + \vec{v}_\perp^2 / \vec{c}^2) . \tag{30}$$

The brief consideration above illustrates the inner processes that occur in space at a submicroscopic level and shows that these processes can be interpreted in the context of a macroscopic formal presentation. At the scale beyond the quantum mechanical formalism two speeds can be additive. Indeed, in the domain of condensed matter physics, which is applicable to the tessellattice, the sound velocity allows variation, thereby affecting the time of movement. However, in the formalism proposed by Minkowski, the speed of light is a strict constant, while time is allowed to change.

In any case, our main purpose has been to find the expression for an effective distance that connects the two interacting objects – the central

mass m_1 and the small orbital mass m_2. Based on the potential energy of Newton's gravity (26) we can write the classical Newtonian gravitational force between these masses as

$$F = G\frac{m_1 m_2}{r'^2} = G\frac{m_1 m_2}{r^2}\left(1+\frac{v_\perp^2}{c^2}\right) \tag{31}$$

and then the appropriate Newton's gravitational potential becomes

$$U = -G\frac{m_1 m_2}{r}\left(1+\frac{v_\perp^2}{c^2}\right). \tag{32}$$

The expressions (31) and (32) slightly alter Newton's law of universal gravitation. In the first approximation we can neglect the second correction term proportional to the ratio $v_\perp^2 / c^2$. However, this term becomes crucial during the experimental verification of a series of subtle measurements. It is this term that introduces the curvature in the formalism of general relativity, and we will discuss it later in this chapter.

MANIFESTATION OF THE CORRECTION $v_\perp^2 / c^2$

The submicroscopic concept, which introduces the corrected version of Newton's law of gravitation (32), allows one to easily solve the problem of the motion of Mercury's perihelion, the deflection of starlight by the Sun, the gravitational redshift of spectral lines, the Shapiro time delay effect as well as other observed gravitational anomalies.

Classical mechanics yields the following equations describing the motion of a body with a mass *m* in the gravitational field induced by a large central mass *M*

$$I = m r^2 \dot{\varphi}, \tag{33}$$

$$E = \tfrac{1}{2} m \dot{r}^2 + \tfrac{1}{2} m r^2 \dot{\varphi}^2 - G \frac{M m}{r} \left(1 + \frac{r^2 \dot{\varphi}^2}{c^2} \right). \tag{34}$$

In Eq. (34) we used the gravitational potential energy (32) with a change of $\upsilon_\perp$ to $r\dot{\varphi}$ because of the choice of a polar system of coordinates. Here, the dot over r and φ implies the differentiation by the proper time t of the body, i.e., t is a natural parameter that is proportional to the path of motion of the body.

The system of equations (33) and (34) are identical to the equations of motion of a body in the Schwarzschild field obtained in the framework of the general theory of relativity. The solution is known (Bergmann, 1976; pp. 214-217)

$$\Delta\varphi = 6\pi G^2 M^2 / \hbar \tag{35}$$

where $\hbar = r \upsilon_\perp = \text{const}$. It is exactly the last term in expression (34), which is responsible for the motion of the perihelion of the planetary orbit (in particular, it was directly observed in Mercury's orbit around the Sun).

Vibrating atoms (ions) located on the surface of a massive object exhibit a gravitational red shift of spectral lines, which is given (Bergmann, 2017; p. 222) in the formalism of general relativity by the expression

$$\delta\nu \cong -\frac{G M}{c^2 r} \nu_0. \tag{36}$$

However, the same expression (40) can be easily derived by considering the motion of a pendulum (Krasnoholovets, 2017; pp. 374-375).

A photon is not a canonical particle, but a quasi-particle, a local excitation of the tessellattice, which migrates in space by hopping from cell to cell (Krasnoholovets, 2017), carrying the polarization state of the cell. A free photon is an elementary massless excitation and hence does not bind with inertons; it cannot experience the radial component of the gravitational field of a massive object (there is no overlapping with the inerton cloud of the mass M). That is why the radial component $-GMm/r$ is absent in the interaction between the massive object and an incident photon. Nevertheless, the tangential component $-GMmr\dot{\varphi}^2/c^2$ associated with the true tangential motion of the photon must still be preserved.

A photon has a kinematic effective mass m because the photon's momentum is $\hbar\vec{k}$ and the notion also follows directly from the "moment of junction" (Krasnoholovets, 2017). That is why the behavior of the photon in the gravitational field of mass M has to be defined by the following pair of equations

$$I = mr^2\dot{\varphi}, \tag{37}$$

$$E = \tfrac{1}{2}m\dot{r}^2 + \tfrac{1}{2}mr^2\dot{\varphi}^2 - G\frac{Mmr\dot{\varphi}^2}{c^2}. \tag{38}$$

Again, the time t is treated as the natural parameter proportional to the photon path, which is essential for the invariance of the theory.

Eqs. (36) and (37) are reduced to the same input equation for the study of the bending of a light ray in the Schwarzschild field of general relativity

$$\left(dr/d\varphi\right)^2 = Q^2r^4/\hbar^2 - r^2 + 2GMr/c^2. \tag{39}$$

The solution to Eq. (38) is well known (Bergmann, 1976; pp. 218-221) and it results in the angle of deviation of the ray from the direct line as expressed by

$$\Delta\varphi \approx 4\frac{GM}{c^2 r}, \tag{40}$$

This deviation has been experimentally verified.

Shapiro's studies (Shapiro, 1964; Shapiro et al, 1968) of the return of signals transmitted from Earth to Venus demonstrated what is known as the gravitational time delay effect. The first tests matched Shapiro's predicted time delay of 200 μs in the presence of a large mass, which was calculated on the basis of the Schwarzschild-Hilbert metric of the Sun. Later on the time delay effect was observed also for several binary pulsars. The result was explained as a general-relativistic delay in the time caused by the nearest mass. However, what would be the reason for such a phenomenon from the submicroscopic point of view?

A path of photons that travel from one planet to the other and return by passing near the Sun can be treated in the framework of a variational problem. Time has to be treated as a natural parameter,

$$t = \int ds / c \tag{41}$$

where ds is the interval length of the path of photons.

A submicroscopic consideration allows a deeper examination into the proper time of migrating photons. Photons have to interact with the mass body as prescribed by the second term of the gravitational potential (32). This interaction with the body's total inerton cloud changes the path of photons near the body according to expression (35), and this be perceived as a local curvature of space. Since real space is organized as the tessellattice of topological balls, curvature of space can easily be illustrated by changes in the geometry of cells of the tessellattice around a massive object. Then the proper time (41) of photons can be written in the form

$$t = \int \frac{ds}{c} = \int \frac{dx}{c} + \int \varphi \frac{dx}{c} \tag{42}$$

and thus the time delay, i.e., the second term in the right hand side of expression (42), appears as

$$\Delta t = \int \varphi(x) \frac{dx}{c} \tag{43}$$

where the angle of deflection is given by (Krasnoholovets, 2014; 2017)

$$\varphi(x) = \frac{4GM}{c^2 \sqrt{R^2 + x^2}}. \tag{44}$$

Here, x is a coordinate along the *X*-axis on which the two masses are located and R is the radius of the Sun that appears near the *X*-axis. Calculating the integral in (43) we find

$$\begin{aligned} \Delta t &= \frac{4GM}{c^3} 2 \left[\ln\left(\chi + \sqrt{1+\chi^2} \right) \Big|_0^{r_1/R} + \ln\left(\chi + \sqrt{1+\chi^2} \right) \Big|_{r_1/R}^{(r_1+r_2)/R} \right] \\ &= \frac{4GM}{c^3} 2 \left[\ln\left(\chi + \sqrt{1+\chi^2} \right) \Big|_0^{r_1/R} + \ln\left(\chi + \sqrt{1+\chi^2} \right) \Big|_{r_1/R}^{(r_1+r_2)/R} \right] \\ &\approx \frac{4GM}{c^3} 2 \ln\left(2 \frac{r_1 + r_2}{R} \right) \approx 2.6 \times 10^{-4} \quad \text{s}, \end{aligned} \tag{45}$$

which is very close to Shapiro's (1964) outcome.

The induction of mass in the space around the body means the appearance of volumetric fractal changes in the corresponding cells of the tessellattice. Namely, cells become contracted in size. This means that the tessellattice is actually contracted around the body. Therefore, in Shapiro's experiment in which the approaching Sun squeezes the surrounding cells of the tessellattice, the photon path between the Earth and Venus increases

owing to additional cells in comparison with the case of a degenerate space where the massive Sun would be absent between these two planets. This situation is in agreement with the general rules of fractal geometry, which make it possible to measure a curve by means of the number of balls that cover it.

Let us choose the size of a topological ball of degenerate space (a cell of the undisturbed tessellattice) to be equal to the Planck's size $l_{\rm P} = \sqrt{\hbar G / c^3} \simeq 1.6 \times 10^{-35}$ m. Covering the photon path with these balls we may evaluate the number of cells N that are responsible for the time delay (45). The number of cells, which form a flat path for photons that hop from cell to cell with a constant velocity c, is

$$N = \frac{1}{l_{\rm P}} \int_0^{r_1+r_2} dx = \frac{r_1 + r_2}{l_{\rm P}} \sim 10^{46}. \tag{46}$$

Thus the length of the flat path is $N \cdot l_{\rm P} \approx 2.17 \times 10^{11}$ m, which is the distance between the Earth and Venus.

Additional cells involved in the path due to the cells' fractal volumetric shrinking caused by the solar mass M, which is owed to the interaction of photons with the gravitational field of mass M through the second term in expression (32), is

$$\Delta N = \frac{1}{l_{\rm P}} \int_0^{r_1+r_2} \varphi(x)\, dx \approx \frac{4GM}{c^2 l_{\rm P}} 2 \ln\left(2 \frac{r_1 + r_2}{R} \right) \sim 5 \cdot 10^{39}. \tag{47}$$

It are these cells that prolong the path of photons and they are responsible for delaying the arrival of the signal; namely, $\Delta N \cdot l_{\rm P} \approx 7.8 \times 10^4$ m, and then the delay is

$$\Delta t = \Delta N \cdot l_{\rm P} / c \approx 2.6 \times 10^{-4} \text{ s}. \tag{48}$$

Thus, the Sun shrinks its surrounding tessellattice, such that the number N of cells in a rectilinear path between the Earth and Venus increases by the value of ΔN. Photons hop with the same speed c from cell-to-cell migrating in the tessellattice. But in the presence of the Sun the number of cells that photons have to pass travelling between the Earth and Venus increases to the value $N + \Delta N$. This is the reason of the gravitational time delay effect in Shapiro's experiment as explained from the submicroscopic viewpoint, which we arrive to by taking into account the peculiarities of fractal geometry which govern the tessellattice.

CURVATURE OF SPACE – A SUBMICROSOCPIC ANALYSIS

Curved space (Wikipedia, with ref. to Papastavridis, 1999) refers to a spatial geometry that is not "flat," where a flat space is described by Euclidean geometry. Curved spaces are generally described by Riemannian geometry. In General relativity, gravity is visualized as curved space. Let us start by considering how a curved space is constructed in conventional geometry.

The major characteristic of a curved space is departure from the Pythagorean theorem, so that in a non-euclidean three-dimensional space:

$$dx^2 + dy^2 + dz^2 \neq ds^2 . \tag{49}$$

Instead, one can describe the 3D space with four dimensions; for this purpose coordinates can be chosen such that

$$ds^2 = dx^2 + dy^2 + dz^2 + dw^2 \tag{50}$$

and the Pythagorean theorem holds again in what is now a 4D space:

$$x^2 + y^2 + z^2 + w^2 = \text{const} . \tag{51}$$

Here, the constant can be positive or negative and is usually defined in the form of $\kappa^{-1}R^2$ where R^2 is positive and $\kappa = \pm 1$.

The constraint κ makes it possible to eliminate the fourth coordinate w introduced by hand. Differentiating Eq. (50) we derive

$$dw = -w^{-1}(xdx + ydy + zdz). \tag{52}$$

Substituting dw from expression (51) into Eq. (49), we get

$$ds^2 = dx^2 + dy^2 + dz^2 + \frac{(xdx + ydy + zdz)^2}{\kappa^{-1}R^2 - x^2 - y^2 - z^2}. \tag{53}$$

Transforming to spherical coordinates $x = r\sin\theta\cos\phi$, $y = r\sin\theta\sin\phi$ and $z = r\cos\theta$ we obtain instead of (53) the metric that describes isotropic and homogeneous space

$$ds^2 = \frac{dr^2}{1 - \kappa r^2 / R^2} + r^2 d\theta^2 + r^2 \sin^2\theta\, d\phi^2. \tag{54}$$

When the constant of curvature $R \to \infty$, space becomes flat, i.e., Euclidean. The same holds when $\kappa \to 0$.

Further optimization of the metric is also possible; the following expression is written for an isotropic and homogeneous space

$$ds^2 = e^{-\lambda(r)}dr^2 + r^2 d\theta^2 + r^2 \sin^2\theta\, d\phi^2, \tag{55}$$

which is reduced to Eucleadian space at $\lambda = 0$. In 3 dimensions, a space is flat when the Ricci tensor $R_{ab} = g_{ab}R$ where g_{ab} is the metric and R is the Ricci scalar; in such a case $\lambda = -\frac{1}{2}\ln(1 - kr^2)$ where $k = R/2$ and the meric (55) becomes

$$ds^2 = \frac{dr^2}{1-kr^2} + r^2 d\theta^2 + r^2 \sin^2\theta \, d\phi^2 . \tag{56}$$

By consideration of curved space, the expressions (49)–(56) show that our attempts to introduce a fourth dimention result in the derivation of a metric in which the radial component has a different behavior inside the sphere, on the surface of the sphere and outside the sphere.

Schwarzschild (1916; Bergmann, 1976; Ch. XIII, pp. 198-203) considered the metric that describes a massive point at rest, possessing spherical symmetry and whose spatial variables do not depend on time *t*, although the time component does play the role of the fourth dimension. Namely, Schwarzschild started from a linear line element

$$\begin{aligned} ds^2 = A(r)\,dt^2 \; + \; 2[B(r)/r]\,\xi_s d\xi^s dt - C(r)\,\delta_{rs} d\xi^r d\xi^s \\ + [D(r)/r^2]\,\xi_s \xi_r \, d\xi^s d\xi^r \end{aligned} \tag{57}$$

where *r* and *s* change from 1 to 3. Introducing peculiar symmetry conditions and keeping the spherical symmetry of the line element ds^2 Schwarzschild reduced the number of variables and came to a metric with the following components:

$$g_{44} = A(r), \quad g_{4s} = 0, \quad g_{rs} = -C(r)\,\delta_{rs} + [D(r)/r^2]\,\xi_r \, \xi_s . \tag{58}$$

By further transformation of the spherical coordinates and keeping particular conditions, Schwarzschild arrived at the metric

$$ds^2 = -\left(1 - r_{\mathrm{S}}/r\right) c^2 dt^2 + \frac{dr^2}{1 - r_{\mathrm{S}}/r} + r^2 d\theta^2 + \sin^2\theta \, d\phi^2 . \tag{59}$$

where the parameter $r_S = 2GM / c^2$ is called the Schwarzschild radius. The Schwarzschild-Hilbert metric is interesting because all the predictions of general relativity, which were tested experimentally, are based on it.

It is important to note that general relativity as a phenomenological therory stops being valid for distances appoaching the particle's de Broglie wavelegth, i.e., the atom size; the critical distance can be taken to be 100 times the atom size, corresponding to the lengthscale where quantum fluctuations dissappear. Therefore, a real point in the differential equations of general relativity is of the size no less than 10^{-8} m.

General relativity and partial relativity both state that the speed of light is constant and cannot be overcome, which is why these theories consider time as a natural parameter, i.e., $l = ct$, where l is the path of the body studied. This results in the introduction of the time component into the metric (59), and is also the reason why the first term can be presented in the form $-(1 - r_S / r) / dr^2$, which looks inverted relative to the second term.

The three last terms in the Schwarzschild metric (59) coincide with those in expressions (54) and (56). Therefore, the peculiarities of the physics of general relativity can be hidden only in the first term that connects the distance r with time t, i.e., really forms the space-time.

In the previous sections we have seen how the submicroscopic consideration of the tessellatice allowed the derivation of the total gravitational potential (32) that takes into account also the tangential component in the interaction of two massive objects. This is possible only when the velocity of inertons, which transfer the gravitational interaction with the speed of light c along the radial line, receive also the tangential component $\upsilon_\perp$ of the orbiting test object. Then the total velocity becomes $\sqrt{\vec{c}^2 + \vec{\upsilon}_\perp^2}$. The interaction of the massive central object with the test orbital one is given by the energy (34).

The tangential correction to Netwon's potential also makes it possible to aptly calculate the gravitational red shift of spectral lines (36); for details see (Krasnoholovets, 2017).

The orbital test body can be represented by a photon; in this case it possesses only the strictly tangential motion along the appropriate equipotential line, which contributes to the energy of interaction (38). The angle of deviation of light under the gravitational potential is found equal to $\Delta\varphi = 4GM/(c^2 r)$ (40), which is also presented in the Schwarzschild metric (58) because of $\Delta\varphi = 2r_S / r$.

The Shapiro test allows a direct interpretation of the motion of photons following the angle of deviation under gravity of the approaching large mass in terms of the fractal contraction of cells of space, resulting in the correct calculation of the time delay of the signal (45), (48).

Thus, the phenomenological consideration in the framework of general relativity, which operates with a natural parameter $l = ct$, suggests that the speed of light c is strictly constant. Then time t has to vary in the presence of gravity.

However, in the framework of the submicroscopic consideration, which is based on the tessellatice as a primary substrate of the space, the relationship $l = ct$ permits an alteration of the speed of light *c*, which can be given by the tangential impact to the carrier of the gravitational interaction, i.e., inerton. Therefore, it is rather the value of *c* that varies in cases where material bodies interact, such that the tangential correction to Newton's gravity is manifested explicitly (as relating to the motion of the perihelion and the gravitational red shift of spectral lines). In this case we can talk about a space-speed connection.

When an orbital body is a photon (the deflection of light), then only the tangential motion of photons occurs leading to the angular deviation of the ray. This is in fact the space-time connection.

The gravitational time delay effect is caused by the traveling of photons along the equipotential lines in the gravitational field of a massive body and fractal contraction of ongoing cells of the space by which the photons have traveled and hence in this situation *c* is preserved, but time *t* and the path length l are increased (48). This is the case of the path-time connection.

In conclusion, all three parameters in the relationship $l = c\,t$ are able to vary, depending on the physical system in question and the inner processes occurring within it.

MANIFESTATION OF INERTONS

The Known Facts

Due to the crucial role of inertons in the submicroscopic theory of gravity, it follows that they must manifest themselves quite widely. In my book (Krasnoholovets, 2017) a number of different experiments conducted in condensed matter, plasma physics, nuclear physics and astrophysics were discussed. Among recent verifications of inerton physics we can mention two studies: 1) an intensification of the technological process of biodiesel production – the first demonstration of the flow mode biodiesel manufacturing using a reactor in which chemical reactions are intensified by a powerful inerton field (Litinas et al., 2020); 2) the transmission of health information signals at a distance using an inerton field channel (Krasnoholovets and Fedorivsky, 2020).

Do other researchers report unusual phenomena that can be explained with inerton physics?

In 1945 a documentary including video materials on the Bell project were seized from the Nazis by Polish intelligence and then passed on to the Soviet secret services (The Bell Project, 2018). In the documentary (The Bell Project, 2018; from 4.0 to 5.24 minutes) one can watch the structure of the Bell and its interior: two metal cylinders rotating at tremendous speed (up to 60,000 rpm) in opposite directions. A concave mirrored spherical surface reflected the emitted radiation because the device appeared to have terrible side effects. Figure 4 shown below is from Y. Abarin's blog and Figures 5 to 7 are screenshots from the mentioned documentary.

Information about this Nazi project of 1944-1945 also leaked to Western countries. Cook (2002) describes the Bell as follows: "it was made out of a hard, heavy metal and was filled with a mercury-like substance, violet in color. This metallic liquid was stored in a tall thin thermos flask a meter high encased in lead three centimeters thick. Each test lasted for approximately one minute."

Figure 4. Phograph of the Bell. From the blog of Yuri Abarin: https://voenhronika.ru/publ/vtoraja_mirovaja_vojna_germanija_khronika/proekt_kolokol_samoe_zagadochnoe_oruzhie_tretego_rejkha_sobrannoe_po_dobiblejskim_tekhnologijam_2020/23-1-0-7897.

Figure 5. Sceenshot (The Bell Project, 2018). The Bell's inner construction: two cylinders rotating in opposite directions and the spherical mirror behind them.

While the Bell emitted its radiation, personnel were kept 150 to 200 meters away from it. Cook further states the following, which is also mentioned in the documentary: "During the tests, the scientists placed various types of plants, animals and animal tissues in the Bell's sphere of influence. In the initial test period from November to December 1944, almost all of the samples were destroyed. A crystalline substance formed within the tissues, destroying them from the inside; liquids, including blood, gelled and separated into clearly distilled fractions."

People exposed to the program complained of ailments: sleep problems, loss of memory and balance, muscle spasms, and an unpleasant metallic taste in the mouth. Five of the seven scientists involved in the project died.

Figure 6. Screenshot (The Bell Project, 2018). No plants are growing around the Bell in a radius of about 30 m in directions to which the concave mirrored spherical surface of the Bell is oriented.

Had the Bell experiment been an attempt by the Nazis to manipulate gravity? In any case, the studies of German researchers during the Nazi time period clearly demonstrated the existence of a new powerful physical field, which was beyond the attention of scientists around the world.

Figure 7. Screenshot (The Bell Project, 2018). All living entities that were places in the emission path of the unknown field decomposed into a kind of white colored mucus without rotting and then felt apart as pieces in several tens of minutes.

Shnoll (2012) demonstrated that certain cosmologocal factors influence the decay of nuclear elements; these factors could be related to solar or even galactic processes, see also (Krasnoholovets, 2017; pp. 407-417).

Certainly, very important studies were conducted by Kozyrev (Kozyrev, 1977; Kozyrev and Nasonov, 1978) and then by other researchers (Lavrentiev et al., 1990). Those researchers demonstrated the presence of a remote influence by several stars (Procyon and others), which affected a signaling sensor made of a resistor incorporated in an electrical bridge circuit. When the sensor was put in the focal volume of the telescope that was tracking these stars, the position of the stars became visible approximately 2 hours before a photon-mediated signal should have detected them. This implies that the detection was mediated by signal carriers whose speed exceeded that of photons.

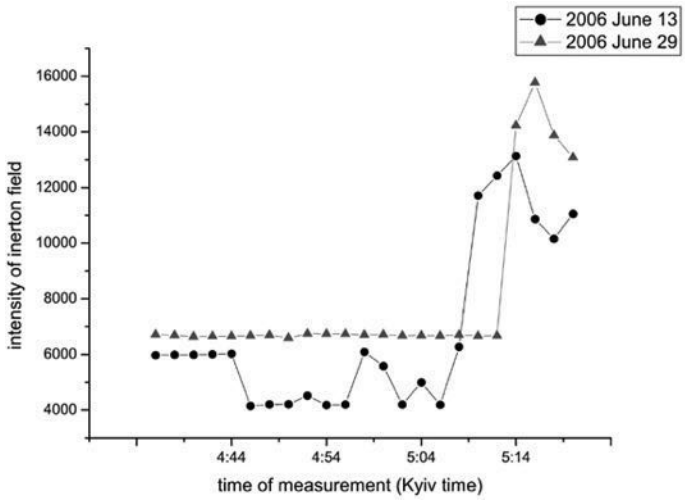

Figure 8. Inerton signals measured at sunrise. The antenna's direction is East-West.

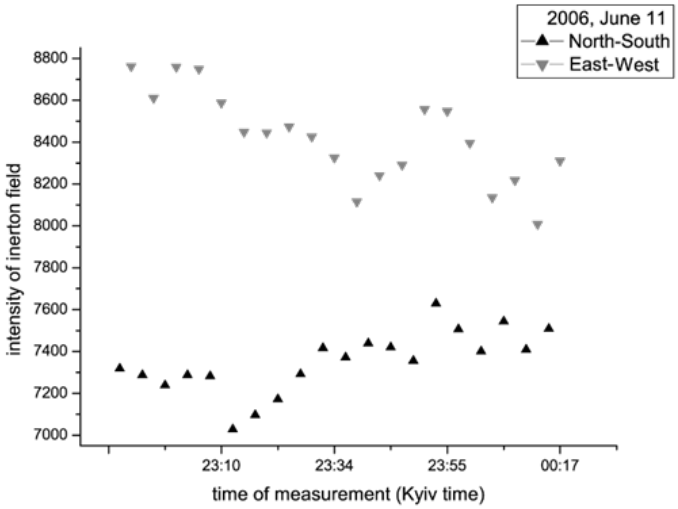

Figure 9. Inerton signals measured after sunset. The antenna was directed along East-West (upper curve) and along North-South (down curve).

In our experiments we recorded inerton signals during sunrise and sunset, and also once during a lunar eclipse. Figures 8 and 9 depict the intensity of inerton signals recorded by a measuring device, where the intensity is represented by the number of particles that interacted with the

antenna per second. The measurements were conducted in a deep concrete basement without windows. The recorded signals in Figures 8 and 9 did not have a time delay like a photon-based signal.

Further studies in a terrestrial lab showed that in the frequency range of a few Hertz to 100 kHz, the dominant contribution is by inertons with frequencies from 2 to 4 kHz (including solar inertons).

Very Recent Observations of Solar Inertons

Much work in the observation of solar anomalies has been done by A. Pugach and his colleagues (Pugach, 2015; 2018; Olenici et al., 2014). The authors monitored the behavior of non-conventional torsion balances, including the torsind, during solar and lunar eclipses (the torsind is a species of ultralight disc torsion balance). They showed that, in addition to reacting to solar and lunar events, the torsion-based measurement devices also experience an influence of the transit of Venus. The reaction of these devices, including Foucault pendulums, to those phenomena either preceded or lagged behind the actual observed event. These perturbations were named "Syzygy effects"; they took place even when the devices were in locations where the eclipse was not visible and even when they were underground. The team also detected an unusual time shift between the response of the devices and the maximum phase of the eclipse.

Based on these observations, it was postulated that that the torsind reacts to non-electromagnetic radiation of an unknown nature, arising in outer space surrounding the Earth. Furthermore, A. Pugach and his colleagues suspected that the origin of the observed effects was the Sun: An unknown radiation bears a torque that impacts the dynamics of the mechanical measurement systems.

Nikolsky and Pugach (2016) described their measurement of a clear response of the Venus transit on June 6, 2012. The observation allowed them to estimate the velocity of an unknown radiation coming from the Sun and impinging on the path Venus-Earth, which they named the 'spiral vortex solar radiation.' The determined value of the signal propagation

speed was 1,990 km·s^{-1}, which strongly implied a new fundamental interaction. They further stated that the main source of the new type of radiation can be attributed to sunspots.

The estimated time of impact of solar 'spirino' microwave radiation (or a radially directed flux of coherent vortex solitons propagating like longitudinal waves) lasted 300-600 s, and the disc rotation angle could reach 7000 degrees (Nikolsky and Pugach, 2015). They observed that in addition to radiation from sunspots, there was a randomly distributed (granulated) background photospheric radiation, and several other types of 'spirino' radiation were also detected. Samples of a pyrite crystal FeS_2 (weight 19.77 g) and thin-layer hidden-grained tuffite (15.5 g) were studied during 60 hours; it was concluded that the samples exposed to the solar active 'spirino' radiation had an additional weight. The observed change of weight varied between 0.002 to 0.02 g with a measurement error of ± 0.00012 g, and the 'spirino' propagation speed was estimated to be 1770 km·s^{-1}. It should be noted that this radiation also has a significant effect on the behavior of water, and by extension, on living beings; it also notably affects the weather and climate system.

So, let us look at the important results obtained by Pugach, Nikolsky and their colleagues from the point of view of submicroscopic physics.

Literature states that sunspots are related to unstable processes and powerful magnetic fields on the surface of the Sun. The Sun is considered as a gaseous plasma with a dense nuclear core. Nevertheless, there are a number of arguments in favor of the fact that the Sun is a condensed matter system (Robitaille, 2013); in particular, it was shown (Krasnoholovets, 2017; Sect. 8.6) that hydrogen, which is the main element of the Sun, is bound via an inerton field in clusters that involve 10^3 to 10^5 of hydrogen atoms and such clusters are tightly packed. This means that the Sun is actually constituted as a peculiar liquid substance.

It is a known fact that ordered thermal cells (thermal columns) are formed on the surface of the Sun. This is a typical situation for a fluid, which appears owing to the phenomenon of Rayleigh-Bénard convection: spontaneous convection occurs in a plane horizontal layer of fluid heated

from below, which results in a regular pattern of convection cells known as Bénard cells.

The average distance between solar columns is about 1800 km, however, the legth of such columns is much longer. Thereofore, owing to the long legth, the columns cannot be homogeneously ordered along the spherical surface of the Sun (the distance between the tops of the nearest columns exceeds the distance between the bottoms of these columns), which means that discontinuities in the ordered network must appear. That is, there should be cavities with a different organization of matter. These cavities are sunspots, i.e., dark spots on the surface of the Sun.

In solar columns convection flows are accompanied by the movement of charged partciles behaving like condensed matter plasma. Charged particles induce magnetic fields, which further regulate the flow of charges.

Surrounding magnetic field fluxes reduce the temperature in regions with sunspots because the fluxes inhibit convection. Sunspots may expand and contract and their diameters ranging from several tens of kilometers to 160,000 km with a middle size of about the diameter of the Earth. Sunspots accompany secondary phenomena such as coronal loops, prominences, and reconnection events. Most solar flares and coronal mass ejections originate in magnetically active regions around visible sunspot groupings (Sunspot, Wikipedia).

Coronal mass ejections (Coronal mass ejection, Wikipedia) eject large quantities of matter and electromagnetic radiation into space above the Sun's surface. The ejected material is magnetized plasma consisting primarily of electrons and protons. Coronal mass ejections reach velocities from 20 to 3,200 $km \cdot s^{-1}$ with an average speed of 489 $km \cdot s^{-1}$. These speeds correspond to transit times from the Sun to the mean radius of Earth's orbit of about 13 hours to 86 days, with about 3.5 days as the average. The ejected mass also varies, with an average of 1.6×10^{12} kg. The frequency of ejections depends on the phase of the solar cycle: from about 0.2 per day near the solar minimum to 3.5 per day near the solar maximum.

In recent studies (Rupke et al., 2020) the authors have found velocity oscillations at frequencies of 3.3 mHz in a big sunspot. The maximum

acoustic power of the observed waves coincided with greatest power of polarization signals, which does not allow the authors to distinguish between the types of acoustic wave mode participating in the oscillations. Discrete velocity amplitudes changed from 47 to 86 ms^{-1}. Oscillatory behavior was also detected in longitudinal field streng at 2.6 and 3.3 mHz. Khomenko and Collados (2015) discuss many problems associated with oscillations and waves in sunspots and in particluar consider possible mechanisms that produce the change of the dominant frequency of waves in the umbra from 3 mHz in the photosphere to 5–6 mHz in the chromosphere.

Note that these were acoustic oscillations of the umbra of sunspots (around 3 mHz), which were recorded by Puhach, Nikolsky and the collaborators in their laboratiores on the Earth. Their 'spiral vortex solar radiation' with fundamental carriers 'spirino' coincides perfectly with inerton waves. Since magneto-hydrodynamic helical plasma tubes arise from sunspots of the photosphere to the chromosphere, the abrupt energy transfer from sunspots to the plasma tubes may be associated with the emission of inerton wavelets, which is a direct mass ejection via the inerton channel. The escape velocty from the Sun is 615 $km{\cdot}s^{-1}$. Pugach and Nikolsky estimated the velocity of the 'spirino' signal as about 1,990 $km{\cdot}s^{-1}$ (in other experiments 1,770 $km{\cdot}s^{-1}$), which falls within the range of velocities of coronal mass ejections of 20 to 3,200 $km{\cdot}s^{-1}$. This means that the emission of inerton wavelets/vortices may occur in parallel with the eruption of plasma clots.

Theoretical Description of the Sunspot's Inertons

When charged particles undergo a quick, non-adiabatic emergence from the condensed matter part to the gaseous plasma atmosphere, they experience an abrupt phase transition. Within the condensed matter part, all the particles' inerton clouds overlap forming a total dense inerton network (Krasnoholovets, 2017). But the passage to the gaseous plasma state leads to them shedding off a part of their inertons, predominantly in the vertical

direction. This vortex motion of a batch of the inerton matter in the framework of a sunspot can be described by the following Lagrangian, written in cylindrical coordinates

$$L = \frac{\mu}{2}\left(\dot{r}^2 + r^2\dot{\varphi}^2 + \dot{z}^2\right) - U(r,\, \dot{\varphi}) + \frac{GM\mu}{z} \tag{60}$$

where μ is the mass of an effective batch of inertons, which is ready to be released at the passing of charged matter to the gaseous plasma atmosphere; r and φ are polar coordinates of the batch of inertons in the sunspot, and z is the coordinate of the batch of inertons in the vertical direction. The first term in the Lagrangian (60) describes the kinetic energy of inertons, the second term $U(r,\, \dot{\varphi})$ characterizes the flat vortex motion of inertons and the third term is the potential energy of the batch of inertons on the gravitational field of the Sun, where the dot represents a time derivative. The rotating potential depicting the planar motion of the batch of inertons in the central field can be chosen in the form

$$U(r,\, \dot{\varphi}) = \frac{\alpha}{2}r^2 + \frac{\beta}{2}r^2\dot{\varphi}\,. \tag{61}$$

In the right hand side of expression (60) the first two members in the brackets and the first member of the potential (61) form a typical central-force harmonic potential, which describes an elastic behavior of the batch of inertons in the sunspot; the second member in the expression (61) includes a dependence on the azimuthal velocity, which means that it depicts the rotation-field potential. The construction of the potential $U(r,\, \dot{\varphi})$ allows us to simulate more correctly the reflection of inertons from the walls of the sunspot, whose cross-section we conditionally consider to be round.

The equations of motion are then written as

$$\frac{d}{dt}\frac{\partial L}{\partial \dot{q}_i}-\frac{\partial L}{\partial q_i}=0\,,\quad i=1,\,2,\,3;\qquad q_1\equiv r,\quad q_2\equiv\varphi,\quad q_3\equiv z\,,$$

or in the explicit form

$$\ddot{r}-r\dot{\varphi}^2+\frac{\alpha}{\mu}r+\frac{\beta}{\mu}r\dot{\varphi}=0\,, \tag{62}$$

$$r\ddot{\varphi}+2\dot{r}\cdot\left(\dot{\varphi}-\frac{\beta}{2\mu}\right)=0\,, \tag{63}$$

$$\ddot{z}+\frac{GM}{z^2}=0\,. \tag{64}$$

These equations can be integrated explicitly or solved numerically at the given initial conditions $r(0)$, $\dot{r}(0)$, $\varphi(0)$, $\dot{\varphi}(0)$, $z(0)$ and $\dot{z}(0)$, and the trajectory of motion can be plotted in coordinates $\{r\cos\varphi,\ r\sin\varphi,\ z\}$. The second equation represents the conservation of angular momentum I:

$$\frac{d}{dt}\left[\mu r^2\left(\dot{\varphi}-\frac{\beta}{2\mu}\right)\right]=0\quad\text{or}\quad I=\mu r^2\left(\dot{\varphi}-\frac{\beta}{2\mu}\right)=\text{const}\,. \tag{65}$$

The solutions to Eqs. (62) and (63) are flat trajectories in the forms of a flower with petals (Krasnoholovets & Gandzha, 2012; Krasnoholovets, 2017; pp. 265-266). The solution to Eq. (64) can be derived from the expression for the total energy along the *Z*-axis

$$E_z=\mu\dot{z}^2/2-\frac{GM\mu}{z}\,, \tag{66}$$

which shows how the velocity of the batch of inertons depends on the distance z from the Sun (Figure 10)

$$\dot{z} = \sqrt{2E_z / \mu}\left(1 + GM\mu / (2E_z z)\right)^{1/2}. \tag{67}$$

That is, the velocity of the batch of inertons, or the inerton vortex, gradually decreases with distance from the Sun.

Such inerton signals were recorded by Pugach and colleagues (Pugach, 2015; 2018; Olenici et al., 2014; Nikolsky and Pugach, 2016). They also observed oscillations of the measuring disc during moments of solar and lunar eclipses, as well as during the time of transit of Venus between the Sun and Earth. Certainly, any movement through the gravitational field must disturb the distribution of cells of the ambient space, i.e., the tessellattice. The absolute value of the gravitational interaction of the Sun and Earth and Venus and Earth are given below

$$\begin{aligned} GM_{\text{Sun}} m_{\text{Earth}} / r_{\text{Sun-Earth}} &= 5.38 \times 10^{32} \text{ J}, \\ Gm_{\text{Venus}} m_{\text{Earth}} / r_{\text{Venus-Earth}} &= 8.72 \times 10^{27} \text{ J}. \end{aligned} \tag{68}$$

As evident from these values (68), the difference is very significant. Since the origin of the gravitational field is dynamic, the standing inerton waves of Venus have to interfere with those coming from the Sun and therefore the total influence on the Earth must increase. In particular, this means that the amplitudes of inerton vortices coming from sunspots of the sunrise, which was in fact measured (Nikolsky & Pugach, 2016).

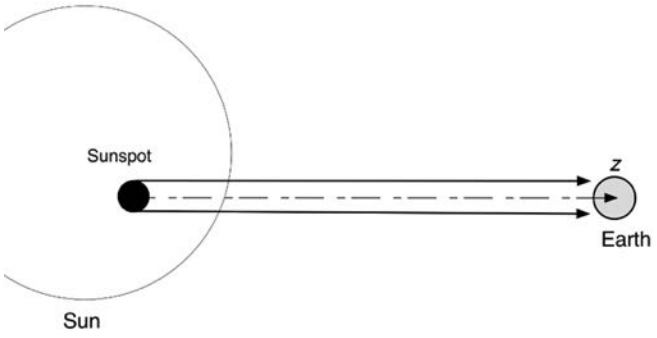

Figure 10. Earth under the inerton radiation from the sunspot of the Sun.

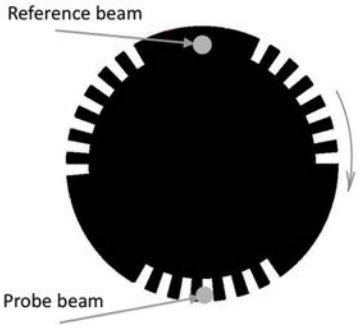

Figure 11. Disk-modulator. The disc transmits the probe and reference light beams in an alternating fashion. It can rotate at different speeds, which sets the frequency of alternating beams. The disk interrupts, or modulates, the beams with its teeth. Modulation is required to distinguish a useful light signal from spurious (daylight) signals.

In times of solar and lunar eclipses a similar situation occurs. Beats in oscillations of the discs, observed by Pugach and colleagues, can be compared with the functioning of a disc-modulator (Figure 11). Periodical interruptions of signals by the teeth of the disc-modulator allow the researcher to detach useful signals from noise.

The simple model presented above gives a basic insight into inerton-related physical processes occurring within sunspots.

DISCUSSION

This paper presents the case that the phenomenon of gravity originates from the constitution of real physical space, i.e., the tessellattice. This substrate is endowed with the property of fractality, allowing for the appearance of contracted (i.e., massive) objects and their motion through the tessellattice. This movement generates spatial excitations – inertons, which provide for an exchange of volumetric fractals, or fragments of mass, between the moving object and the surrounding tessellattice. These local deformations of space induce a deformation potential around the massive object, which we perceive as the object's gravitational potential. Inertons can be released from the object's inerton cloud and the effects

caused by these inertons allow them to be observed and studied. Several phenomena directly related to the manifestation of inertons have been considered in previous sections.

What consequences do we get from the fact of the existence of inertons? First of all inertons are able to change the mass of the object under consideration. The object absorbing external inertons increases its mass; it was demosntarted in a number of experiments conducted in condensed matter physics (Krasnoholovets, 2017; Ch. 5).

The heated body grows in mass. It was demonstrated in the experimen of Peter Fred (2014), whose experiment is shown in Figure 12. A 489 gm hollow copper hemisphere hovers to 200–240 °C by a heat element. In about 5 minutes and the gravitational mass of the hemisphere increased by 9.6 %, or by 47 gm. After 400 s of cooling time, the gravitational mass decreased by 2.0%, or 21 gm.

When a 1068 gm hollow copper sphere initially was at room temperature and then the sphere began to cool using an ice-filled copper container, the sphere's weight or gravitational mass decreased by 4.9 % or 54 gm in 5 minutes.

Here is desription of my simple exmeriment. A stainless steel pan filled with tap water at a room temperature had a weight 1.80 kg. The pan was heated to 100°C and its weight was immediately measured: 1.722 kg (an accuracy of the electronic scales was ±5 gram). So, the weight of the pan with water decreased by 4.7%.

Why did the weight of the Peter Fred's systems and mine change? Because the atoms of the system (Fred's hemisphere and sphere and my pan with water) began to oscillate with larger amplitudes when they are heated. This means that the systems more actively emit not only photons of the infrared spectrum, but also inertons. The flow of inertons, i.e., carriers of mass, directed against the earth's gravitational field caused a clear antigravity effect and the weight dropped. When Fred's sphere cooled, its atoms began to oscillate with smaller amlitudes and hence a flow of emitted ineterons became weaker even in comparison with the initial thermodynamic equilibrium state. That is white the sphere experinced a stronger gravitational attraction to the earth.

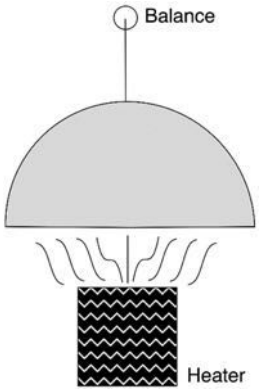

Figure 12. Heater warms the cooper hemisphere.

What are the implications of the existence of inertons? For one, they eliminate the topic of gravitational waves postulated by general relativity, whose existence has been doubted by other researchers as well. In particular, Loinger and Marsico (2016) noted: "The undulatory solutions of the Einstein homogeneous field equations do not possess a true, generally covariant energy-tensor which is different from zero, i.e., they do not posses a physical reality. In general relativity (GR) the speeds of the reference frames are arbitrary, from zero to infinite; consequently, the same thing happens for the speeds of the undulatory metric tensors. The value *c* is not unique, as the astrophysical community believes." Crothers (2016) wrote: "…the consequential claims of detecting gravitational waves, are proven false. The apparent detection by the LIGO-Virgo collaborations is not related to gravitational waves or to the collision and merger of black holes." Besides, in the critical papers in which the protocols of LIGO-Virgo collaborations were investigated in detail (Creswella et al., 2017; Jackson et al., 2019), the authors state that during the detection of gravitational waves by LIGO and Virgo of 2015, the signal was indistinguishable from noise.

The submicroscopic consideration makes it possible to draw a negative conclusion about the Friedmann–Lemaître–Robertson–Walker metric. This metric is non-physical because the spatial components of the metric depend on time

$$ds^2 = a^2(t)(dx_1^2 + \sin^2 x_1\, dx_2^2 + \sin^2 x_1 \sin^2 x_2\, dx_3^2) + M^2(x_1, x_2, x_3, t)\, dt^2 \quad (69)$$

where $M^2(x_1,\ x_2,\ x_3,\ t)$ is a function (not a mass); $a(t)$ is proportional to the radius of curvature of space, which by Friedmann's idea depends on time. Hence the radius of curvature *R*, which is now a scalar factor $a(t)$, can artificially change over time.

From the mathematical point of view, space-time is represented by ordered sequences of topologically closed Poincaré sections of the primary space (Bounias, 2000; Bounias & Krasnoholovets, 2003). These mappings are constrained to provide homeomorphic structures serving as frames of reference in order to account for the successive positions of any object present in the system. Mappings from one to the next section involve morphisms of the general structures, representing a continuous reference frame, and morphisms of objects present in various parts of this structure. The combination of these morphisms provides space-time with the features of a nonlinear generalized convolution. Then the notion of pure time allows the following definition: in any 4D space, the ordered sequence of closed intersections $\{(E^d)_{d<4}\}$, with respect to mappings of members of $\{(E^d)_{d<4}\}_i$ into $\{(E^d)_{d<4}\}_j$, provides an orientation accounting for the physical arrow of time.

In the language of physics, this means that time is a set of consecutive states of the system in question. In the framework of this definition, the metric (69) allows the set of consecutive states to be the set of consecutive states. This is worse than a tautology because it permits the existence of numbers that depend on numbers. That is, a curvature (a scalar) R_1 dependens on R_2, and R_2 depends on R_3 and R_4, and so forth. In other words, the number 5 depends on the number 3; the number 7 depends on number 1, number 5, number 10, etc; the number $\pi = 3.1415...$ was perceived by my grandfather as the number $\pi = 2.0537...$, but my grandchildren will know it as $\pi = 5.4518...$ It quickly becomes evident that such a situation is completely absurd.

Moreover, the metric (69) is not able to describe any of the crucial tests of general relativity, which have been performed using the Schwarzschild-Hilbert metric. Therefore, physicists must discard the metric (69) as untenable.

Since the Friedmann–Lemaître–Robertson–Walker metric is not real, the conclusions based on it are false; in particular, this implicates the Big Bang theory as being false as well. What exploded? What was the reason for this explosion? These are examples of questions that cannot be answered on this basis.

Astrophysicists still continue to hypothesize about the origin of dark matter and dark energy, and the reason for inflation of the universe. The tendency is not to describe known empirical phenomena, but rather to maintain the available mathematical consistency of the theory itself despite having to take into account conflicting observations. It is strongly evident that general relativity is unable to answer these questions, as it fails to describe even the simple interaction of two distant point masses! Nevertheless, most physicists continue to work within the relativistic formalism, causing them to walk in a vicious circle.

At the same time, the submicroscopic deterministic concept gave a simple yet elegant solution to the dark matter problem (Krasnoholovets, 2011; 2017, pp. 391–398): in the gravitational interaction of two massive objects, their inerton clouds overlap and the resulting convergence creates an additional term for the interaction between the massive objects, which must be taken into consideration. Dark energy is explained by a gradual drop in pressure of the body of the spherical universe (constitued of topological balls) as it approaches the periphery where the speed of light c decreases, giving rise to the illusion of an expanding universe (Krasnoholovets, 2017, pp. 402–406). Furthermore, a "black hole" is naturally materialized as a super dense area of inertons belonging to rotating masses in the barycentre of a galaxy (Krasnoholovets, 2017, pp. 398–401).

We maintain that the submicroscopic deterministic concept both clarifies and gives greater detail to our understanding of the cosmos.

CONCLUSION

The considerations presented in this chapter focus on the idea that the universe is constituted by an eternal substrate that shares both discrete and continuum properties. This physical space has the structure of a tessellattice, with mass appearing as a local fractal volumetric deformation of a cell. The interaction of a moving particle-like deformation with the surrounding tessellattice involves a fractal decomposition process that supports the existence and properties of inerton clouds as associated to particles.

A moving particle together with its inerton cloud is mapped to the quantum mechanical formalism as a particle's wave ψ-function. On the other hand, inertons oscillating around a massive object behave like standing spherical waves, establishing a peculiar landscape in the tessellatice around the object. In the mean-field approximation this landscape looks like Newton's gravitational potential $-GM/r$.

When a test mass m possessing a tangential velocity $v_{\perp}$ appears in the vicinity of a central object with mass M, it introduces an additional term to Newtonian gravity proportional to $v_{\perp}^2/c^2$. The total gravitational potential of the interacting central object and test mass $-GMm/r\cdot(1+v_{\perp}^2/c^2)$ makes it possible to solve all the problems predicted by general relativity.

The submicroscopic consideration further makes it possible to understand the manifestation of wave properties of massive bodies in the solar system, as well as to reduce the Casimir effect to the exhibition of quantum gravity (Krasnoholovets, 2017; Ch. 8). Moreover, inerton physics has allowed us to solve major problems of astrophysics and cosmology, such as dark matter, dark energy, "black holes" and mystical solar radiation effects.

Further activity in support of the submicroscopic concept of gravity described above would be the foundation of the first inerton observatory.

By studying inerton rays, the inerton observatory will provide a constant stream of data about the behavior of massive objects, including but not limited to the Sun, planets, stars, and galaxies. Specifically, this would be done by studying the intensity and spectrum of inerton signals, the direction of their arrival, the degree of signal homogeneity, as well as through measurement of the speed of batches and free inertons. Observations of solar inertons will be of major importance, due to their direct influence on weather conditions on Earth, human behavior and health.

Another important conclusion from the discovery of inertons is that they allow us to take the problem of studying antigravity quite seriously.

REFERENCES

Bergmann, P. G. (1976). *Introduction to the Theory of Relativity*, 2nd edition, Dover Publication, Inc., New York.

Bounias, M. (1900). *La Création de la vie: De la matière à l'esprit*, Editions du Rocher, Paris.

Bounias, M. (2000). The theory of something: a theorem supporting the conditions for existence of a physical universe, from the empty set to the biologicalself, in (Daniel M. Dubois, Ed.): CASYS'99 Int. Math. Conf., *Int. J. Comput. Anticipatory Systems*, 5, 11-24.

Bounias, M., & Krasnoholovets, V. (2003). Scanning the structure of ill-known spaces. Parts 1-3. Eds.: Feng, L., B. P. Gibson and Yi Lin, *Kybernetes: The Int. J. Systems & Cybernetics* 32, No. 7/8, 945–1020. arXiv:physics/0211096, arXiv:physics/0212004, arXiv: physics/0301049.

Christianto, V., Krasnoholovets, V., & Smarandache, F. (2019). The wave behavior of quantum systems and the submicrosocpic concept of the microworld, in *Old Problems and New Horizons in World Physics. Archaeology of Modern Physics.* Editors: V. Christianto, V. Krasnoholovets and F. Smarandache. Nova Science Publishers Inc., New York, pp. 93-109.

Clifford, W. K. (1882). On the space-theory of matter, in *Mathematical Papers by William Kingdom Clifford*, Ed.: Robert Trucker, Macmillan and Co., London pp. 21–22.

Cook, N. (2002). *Hunt for Zero Point. Inside the Classified World of Antigravity Technology*, Broadway, pp. 191-194.

Coronal mass ejection, *Wikipedia*, https://en.wikipedia.org/wiki/Coronal_mass_ejection.

Creswella, J., von Hauseggera, S., Jackson, A. D., Hao Liu, Naselsky, P. (2017). On the time lags of the LIGO signals. *J. Cosmology and Astroparticle Phys*., Volume 2017, 017.

Crothers, S. J. (2016). A critical analysis of LIGO's recent detection of gravitational waves caused by merging of black holes, vixra.org/abs/1603.0127.

Fred, Peter. (2014). *Is the sun's warmth gravitationally attractive?* https://www.researchgate.net/publication/242608026_Is_the_sun%27s_warmth_gravitationally_attractive?enrichId=rgreq-2ff8aa63c59e9ae53a9278ab56ba6585-XXX&enrichSource=Y292ZXJQYWdlOzI0MjYwODAyNjtBUzoxMDIzODE3NjUyNjc0NzNAMTQwMTQyMTEyNDAyMg%3D%3D&el=1_x_2&_esc=publicationCoverPdf.

Jackson, A. D., Hao Liu, & Naselsky, P. (2019). Noise residuals for GW150914 using maximum likelihood and numerical relativity templates, *J. Cosmology and Astroparticle Phys.*, Volume 2019, 014.

Khomenko, E., & Collados, M. (2015). Oscillations and waves in sunspots, *Living Reviews in Solar Physics* 12, Article number: 6.

Koshlyakov, N. S., Gliner, E. B., & Smirnov, M. M. (1970). *Partial Differential Equations of Mathematical Physics*, Vysshaya shkola, Moscow; p. 184; in Muscovite.

Kozyrev, N. A. (1977). Astronomical observations by means of the physical properties of time, in: *Flaring Stars: Proceedings of the Symposium Dedicated to the Opening 2.6-m Telescope of the Byurakan Astrophysical Observatory*, Byurakan, October 5–8, 1976. Yerevan, pp. 209–227; in Muscovite.

Kozyrev, N. A., & Nasonov, V. V. (1978). A new method of determination of trigonometric parallaxes on the basis of measurements of difference

between apparent and visible position of stars, in: *Asronometry and Celestial Mechanics*, Akademiya Nauk SSSR, Moscow, Leningrad, pp. 168–179; in Muscovite.

Krasnoholovets, V. (2011). Dark matter as seen from the physical point of view, *Astrophysics and Space Science* 335, No. 2, 619-627.

Krasnoholovets, V. (2014). On the gravitational time delay effect and the curvature of space, *Int. J. Computing Anticipatory Systems* (Edited D. Dubois) 27, 137–147.

Krasnoholovets, V. (2017). *Structure of Space and the Submicroscopic Deterministic Concept of Physics*, Apple Academic Press, Oakville, Canada; Waretown, USA.

Krasnoholovets, V. (2019). Magnetic monopole as the shadow side of the electric charge, in *Journal of Physics Conference Series* 1251:012028 (*Conference Proceeding* SEARCH FOR FUNDAMENTAL THEORY: The IX International Symposium Honoring French Mathematical Physicist Jean-Pierre Vigier (12-14 August 2018, Liege), Eds.: R. L. Amoroso, D. Dubois.

Krasnoholovets, V., & Fedorivsky, V. (2020). Transmission of wellness information signals using an inerton field channel, *European Journal of Applied Physics* 2, No. 6, 1-8.

Krasnoholovets, V., & Gandzha, I. (2012). A sub microscopic description of the formation of crop circles, *Chaotic Modeling and Simulation* 2, 323-335.

Krasnoholovets, V., & Tane, J.-L. (2006). An extended interpretation of the thermodynamic theory including an additional energy associated with a decrease in mass, *Intern. J. Simulation and Process Modelling* 2, Nos. 1/2, 67-79; also arXiv:physics/0605094.

Lavrentiev, M. M., Yeganova, I. E., Lutset, M. K., & Fominykh, S. F. (1990). About distant influence of stars on a resistor. *Proceed. Acad. Scien. USSR* 314(2), 352–355; in Muscovite.

Lavrentiev, M. M., Gusev, V. A., Yeganova, I. A., Lutset, M. K., & Fominykh, S. F. (1990). About the registration of an actual position of the Sun, *Proc. Acad. Sci. USSR* 315(2), 368–370; in Muscovite.

Litinas, A., Geivanidis, S., Faliakis, A., Courouclis, Y., Samaras, Z., Keder, A., Krasnoholovets, V., Gandzha, I., Zabulonov, Y., Puhach, O., & Dmytriyuk, D. (2020). Biodiesel production from a high FFA feedstock with a chemical multifunctional process intensifier, *Biofuel Research Journal* 7, No. 2, 1143-1177; https://www.biofueljournal.com/article_107960.html.

Nikolsky, G. A., & Pugach, A. F. (2015). On definition of components of a penetrating solar field. The reason that ensured civilization to be existing, in *New on the impact of the sun on the environment*, Ed.: G. A. Nikolsky, Lambert Academic Publishing, Saarbrucken, Ch. 4, pp. 72-88; in Muscovite; https://www.researchgate.net/publication/278022296_K_opredeleniu_komponent_solnecnogo_pronikausego_pola_Pricina_obespecivsaa_susestvovanie_civilizacii.

Nikolsky, G., & Pugach, A. (2016). Gravitational lensing of spiral vortex solar radiation by Venus. *Open Access Library J.* 3, 1-11, https://www.scirp.org/journal/PaperInformation.aspx?PaperID=69722.

Loinger, A., & Marsico, T. (2016). A detailed confutation of LIGO's statements on the 150914-signal, *ReserachGate*, https://www.researchgate.net/publication/301542915_A_DETAILED_CONFUTATION_OF_LIGO'S_STATEMENTS_ON_THE_150914-SIGNAL.

Olenici, D., Pugach, A. F., Cosovanu, I., Lesanu, C., Deloly, J.-B., Vorobyov, D., Delets, A., & Olenici-Craciunescu, S.-B. (2014). Syzygy effects studies performed simultaneously with Foucault pendulums and torsinds during the solar eclipses of 13 November 2012 and 10 May 2013, *Int. J. Astronomy and Astroph*. 4, 39-53.

Papastavridis, J. G. (1999). *Tensor Calculus and Analytical Dynamics*, Boca Raton: CRC Press, pp. 211-218.

Poincaré, H. (1906). Sur la dynamique de l'électron, *Rendiconti del Circolo matematico di Palermo* 21, 129–176; also: Oeuvres, t. IX, 494–550 (in Muscovite translation: Henri Poincaré. Selected Transactions in Three Volumes, Vol. 3. Ed.: Bogolubov, N. N., Nauka, Moscow, 1974, pp. 429–486).

Poincaré, H. (1908). La Dynamique de l'électron, *Revue générale des Sciences pures et appliquées* 19, 386–402. (in Muscovite translation:

Henri Poincaré. Selected Transactions in Three Volumes, Vol. 3. Ed.: Bogolubov, N. N., Nauka, Moscow (1974); pp. 487–515).

Pugach, A. F. (2015). Diurnal variations and spikes by the torsind registered and their impact on the accuracy of G measurement. *Int. J. Astronomy Astrophys*. 5, 28–37.

Pugach, A. (2018). Unexplained temporal effects recorded by the torsind at syzygies. *J. Adv. Phys.* 15, 5951-5969.

Robitaille, P.-M. (2013). Forty lines of evidence for condensed matter – the Sun on trial: liquid metallic hydrogen as a solar building block, *Progress in Physics* 4, 90–142.

Rupke, R., Labonte, B. J., & Mickey, D. L. (2000). Observational study of sunspot oscillations in Stokes I, Q, U, and V, *Solar Physics* 191(1), 97–128.

Schwarzschild, K. (1916). Über das Gravitationsfeld eines Massenpunktes nach der Einstein'schen Theorie, *Sitzungsberichte der Königlich Preussischen Akademie der Wissenschaften* 1, 189–196 (English translation: On the gravitational field of a mass point according to Einstein's theory arXiv: physics/9905030).

Shapiro, I. I. (1964). Fourth test of general relativity, *Phys. Rev. Lett*. 13(26), 789–791.

Shapiro, I. I., Pettengill, G. H., Ash, M. E., Stone, M. L., Smith, W. B., Ingalls, R. P., & Brockelman, R. A. (1968). Fourth test of general relativity: Preliminary results, *Phys. Rev. Lett*. 20(22), 1265–1269.

Shnoll, S. E. (2012). *Cosmophysical Factors in Stochastic Processes*, American Research Press, Rehoboth, New Mexico.

Sunspot, Wikipedia https://en.wikipedia.org/wiki/Sunspot.

ter Haar, D. (1974). *Elements of Hamiltonian Mechanics*; Moscow: Nauka, 1974, p. 173 (Muscovite translation from the Second edition, Pergamon Press, 1971).

The Bell Project (2018). *From the archaives; in Muscovite*: https://www.youtube.com/watch?v=NwdJQKvVIhc.

Wikipedia, Curved space, https://en.wikipedia.org/wiki/Curved_space.

SCH